OKU Fen Bilimleri Enstitüsü Dergisi
6(1): 854-872, 2023

OKU Journal of The Institute of Science and Technology, 6(1): 854-872, 2023

Osmaniye Korkut Ata Üniversitesi Fen Bilimleri Enstitüsü Dergisi

Osmaniye Korkut Ata University Journal of The Institute of Science and Technology

Destekleyici Elektrolitin, Süperkapasitör için Elektrokimyasal Biriktirilmiş PEDOT/ERGO Elektrotlarının Kapasitans ve Empedans Özellikleri Üzerindeki Etkisi

Tolga KARAZEHİR[1*]

[1] Adana Alparslan Türkeş Bilim ve Teknoloji Üniversitesi, Mühendislik Fakültesi, Enerji Sistem Mühendisliği Bölümü , 01250 Sarıçam, Adana, Türkiye

[1] https://orcid.org/0000-0002-2795-3675
* Corresponding author: tkarazehir@atu.edu.tr

Araştırma Makalesi

Makale Tarihçesi:
Geliş tarihi: 12.12.2022
Kabul tarihi: 05.02.2023
Online Yayınlanma: 10.03.2023

Anahtar Kelimeler:
Poli(3,4-etilendioksitiyofen)
Grafen
Süperkapasitör

ÖZ

Bu çalışmada, süperkapasitörler için Poli(3,4-etilendioksitiyofen) /elektrokimyasal olarak indirgenmiş grafen oksit (PEDOT/ERGO) elektrotların enerji depolama yetenekleri incelenmiştir. PEDOT/ERGO elektrotları, grafen oksidin elektrokimyasal olarak indirgenmesini içeren iki aşamalı basit bir elektrokimyasal yöntem kullanılarak ve ardından PEDOT, farklı elektrolit çözeltilerinde ERGO üzerine elektrokimyasal olarak biriktirilerek üretildi. 0,1 M lityum perklorat/asetonitril ($LiClO_4$/ACN), tetraetilamonyum tetrafloroborat/asetonitril (Et_4NBF_4/ACN) ve tetrabütilamonyum hekzaflorofosfat/asetonitril (Bu_4NPF_6/ACN) dâhil olmak üzere farklı elektrolit sistemlerinde üretilen PEDOT/ERGO elektrotlarının, döngüsel voltametri (DV), galvanostatik yükleme boşalma testi (GYB) ve elektrokimyasal empedans spektroskopisi (EES) gibi elektrokimyasal teknikler PEDOT/ERGO elektrotlarının elektrokimyasal özelliklerini araştırmak için kullanıldı. Elektrolit tipinin elektrokimyasal sonuçlar üzerinde önemli bir etkisi vardır. $LiClO_4$/ACN'de üretilen PEDOT/ERGO, yüksek spesifik kapasitans (Csp) ve düşük yük transfer direnci (Rct) gösterdi. Sonuçlara göre spesifik kapasitans değerleri şu sırayla azalmaktadır; $LiClO_4$ için 26,48 $mFcm^{-2}$, Et_4NBF_4 için 20,58 $mFcm^{-2}$, Bu_4NPF_6 için 8,96 $mFcm^{-2}$.

Effect of Supporting Electrolyte on Capacitance and Impedance Properties of Electrodeposited PEDOT/ERGO Electrodes for Supercapacitor

Research Article

Article History:
Received: 12.12.2022
Accepted: 05.02.2023
Published online: 10.03.2023

Keywords:
Poly(3,4ethylenedioxythiophene)
Graphene
Supercapacitor

ABSTRACT

In this study, the ability of Poly (3,4-ethylenedioxythiophene)/electrochemically reduced graphene oxide (PEDOT/ERGO) electrodes for supercapacitors to store electrical energy is studied. PEDOT/ERGO electrodes are produced using a simple two-step electrochemical method that involves electrochemically reduction of graphene oxide, and then PEDOT is electrochemically deposited onto the ERGO in different electrolyte solutions. Electrochemical techniques such as cyclic voltammetry (CV), galvanostatic charge discharge (GCD), and electrochemical impedance spectroscopy (EIS) are utilized to investigate the electrochemical characteristics of PEDOT/ERGO electrodes produced in different electrolyte systems including 0.1 M lithium

perchloride/acetonitrile ($LiClO_4$/ACN), tetraethylammoniumtetrafluoroborate/acetonitrile (Et_4NBF_4/ACN), and tetrabutylammonium hexaflorophosphate/acetonitrile (Bu_4NPF_6/ACN). The electrolyte type has a significant impact on electrochemical results. PEDOT/ERGO manufactured in $LiClO_4$/ACN demonstrates a high specific capacitance (C_{sp}) and low charge transfer resistance (R_{ct}). According to results, the C_{sp} value is decreased in the following order; 26.48 $mFcm^{-2}$ for $LiClO_4$, 20.58 $mFcm^{-2}$ for Et_4NBF_4, 8.96 $mFcm^{-2}$ for Bu_4NPF_6.

To Cite: Karazehir T. Effect of Supporting Electrolyte on Capacitance and Impedance Properties of Electrodeposited PEDOT/ERGO Electrodes for Supercapacitor. Osmaniye Korkut Ata Üniversitesi Fen Bilimleri Enstitüsü Dergisi 2023; 6(1): 854-872.

1. Introduction

Clean and sustainable energy is required due to the limitations of energy produced from renewable sources and the contamination of the air by the usage of fossil fuels. To solve this problem, renewable energy sources like solar and wind have been the focus of scientific investigation into the development of innovative technologies for the effective conversion and storage device (Albadi and El-Saadany, 2010; Safari, 2011; Meroni, et al. 2018). Using solar energy is unquestionably the better option. To convert solar energy into electricity, a variety of solar cells, including perovskite, dye-sensitized, and silicon cells have been used. Important factors include storing power from multiple sources and guaranteeing the regularity, viability, and dependability of energy networks (Ranjan, et al., 2011; Liu, et al., 2013; Hu, et al., 2016). Many energy storage systems continue to fall below the required criteria and efficiency for acquiring energy storage. Hybrid electric vehicles (HEVs) are unquestionably green technology automobiles for the future, and will aid in the reduction of conventional fuel usage (Nelson, 2000; Cairns and Albertus, 2010). The high power and energy density energy storage devices, such as supercapacitors and high-capacity batteries are best candidate for HEVs based transport systems (Smith, et al., 2002; Su, 2014). Although Batteries have the highest energy densities of the two storage alternatives, they have also the disadvantages of poor power density and cycle stability. Supercapacitors, however, have a low energy density while having a high power density and cyclic stability. This indicates that none of these two energy storage systems can, by itself, satisfy their respective needs for high energy and power density capacity and cycle stability (Xu and Zhou, 2015; Choudhary, et al., 2020). In contrast to batteries, supercapacitors store electrical charge in electrical double layers that develop at the interface of the electrode and electrolyte. They are now used in industrial energy/power management systems, consumer electronics, and memory backup systems. (Bang, et. al. 2013; Huet, et al., 2022; Landers, et al. 2022). Some of the most important characteristics of an electrode material for a high-performance supercapacitor are its conductivity, distribution of optimal pore size, ease of production, specific surface area, corrosion resistance, and affordability (Naoi, et al., 2013; Yang, et al., 2015; Wang, et al., 2017; Wang, et al., 2018). Hence, establishing supercapacitors as more effective energy storage devices than batteries requires careful consideration of electrode materials and optimizing their design. The extended cycle life of supercapacitors, high

power density, low charging time, and safety have made them more popular during the last decade. Electrochemical double layer capacitance (EDLC) and pseudocapacitance are the two most common energy storage processes in supercapacitors; EDLC stores energy by ion accumulation, whereas pseudocapacitance stores energy through a surface redox reaction (Jiang, et al., 2013; Hashim, et al., 2017). All conducting polymers rely on a faradic charge storage mechanism to perform their function, giving rise to capacitance names as pseudocapacitance (Wang, et al., 2017). A pseudocapacitor typically stores more charges than EDLC due to the most of the charge storage via faradaic redox reaction (Snook, et al. 2011). Therefore, conducting polymers use in supercapacitors due to high stability with high pseudocapacitance, and easy synthesis (Vonlanthen, et al., 2014; Athira, et. al, 2017; Wang, et al., 2017). In addition, conducting polymers have a low band gap (1-3 eV). They are quickly doped and undoped and have a good surface structure and rapid charge kinetics (Ryu, et al., 2004). Conducting polymers have plastic qualities and may therefore be readily manufactured, particularly as thin films (Arbizzani, et al., 1996). Significant research has been conducted on the manufacture of a poly(3,4-ethylene dioxidethiophene) (PEDOT) based nanocomposite as an important conducting polymer type, as well as its use as an active material for electrochemical supercapacitors (Ryu, et al., 2004; Sonia, et al., 2013; Ahmed and Rafat, 2018; Hu, et al., 2019). Studies have shown that PEDOT is much more stable than competing conducting polymers. There is growing interest in using it in supercapacitors and electrochromic devices, and it looks to be among the best stable conducting polymers presently available (Murugan, et al., 2006). Due to their great surface area and outstanding electrical and chemical characteristics, carbon-based electrodes are widely employed to build conducting polymer/carbon based composite for energy storage device (Liu, et al., 2017; Huang, et al., 2019; Wang, et al., 2021).

In this research, electrochemically reduced graphene oxide (ERGO) was generated by reducing graphene oxide. PEDOT was synthesized onto the ERGO-modified glassy carbon electrode in different electrolyte environments (Bu_4NPF_6/ACN, Et_4NBF_4/ACN, and $LiClO_4$/ACN) to investigate the effect of electrolyte type on the charge storage performance of the obtained PEDOT/ERGO. The findings showed that electrolyte type had a significant effect on capacitance of produced PEDOT/ERGO electrodes. The PEDOT/ERGO electrode doped with a ClO_4^{-1} anion had the greatest specific capacitance.

2. Material and Methods

3,4-ethylenedioxythiophene (EDOT), tetraethylammonium tetrafluoroborate (Et_4NBF_4, 99%), tetrabutylammonium hexaflorophosphate (Bu_4NPF_6, 99%), lithium perchloride ($LiClO_4$, 99%) acetonitrile (ACN, anhydrous, 99,8%), sodium phosphate monobasic (NaH_2PO_4) and sodium phosphate dibasic (Na_2HPO_4) were purchased from Sigma Aldrich and used as received. Graphene oxide (GO) was also purchased from Sigma Aldrich. An IviumStat potentiostat/galvanostat was used for all of the electrochemical tests. The GCE (3 mm diameter) was prepared for the tests by first being

polished with 0.05 m alumina suspension, then sonicated in acetone and doubly distilled water, and then dried at ambient temperature. Two hours of ultrasonic exfoliation of commercial GO powder in deionized water yielded a GO aqueous solution (1.0 $mgmL^{-1}$). The GO film was prepared by drop-casting 8 µL of GO suspension solution (1.0 $mgmL^{-1}$) over the surface of pre-cleaned GCE and letting it cure under an IR light for 15 minutes. Electrochemical reduction of GO film was performed by cyclic voltammetry. GO was electrochemically reduced to ERGO a using cyclic voltammetry in the potential range 0-(-1.5) V in N_2 saturated 0.1 M Phosphate Buffered Saline (PBS pH 7) solution for 15 consecutive cycles at a scan rate of 0.05 Vs^{-1}. PEDOT/ERGO/GCE electrode was prepared by the polymerization of EDOT ($[EDOT]_0$=10 mM) in three-electrode cell configuration using ERGO/GCE as a working electrode, Pt wire as counter electrode, and Ag/AgCl (3,5 M KCl) electrode as a reference electrode via cyclic voltammetry in three different electrolytes 0.1 M Et_4NBF_4/ACN, Bu_4NPF_6/ACN, $LiClO_4$/ACN for 10 successive cycles in the potential range from -1.0 to 1.5 V at a scan rate of 0.1 Vs^{-1}. The EIS measurements at OCP were taken with an AC signal amplitude of 10 mV and a frequency range of 10 mHz to 100 kHz. Between 400 and 4000 cm^{-1}, PEDOT/ERGO structures were examined using Fourier-transform infrared attenuated total reflectance spectroscopy (FTIR-ATR; Bruker Vertex 70 ATR). The Quanta FEG 250 microscope was used for scanning electron microscopy (SEM) imaging research.

3. Results and Discussions

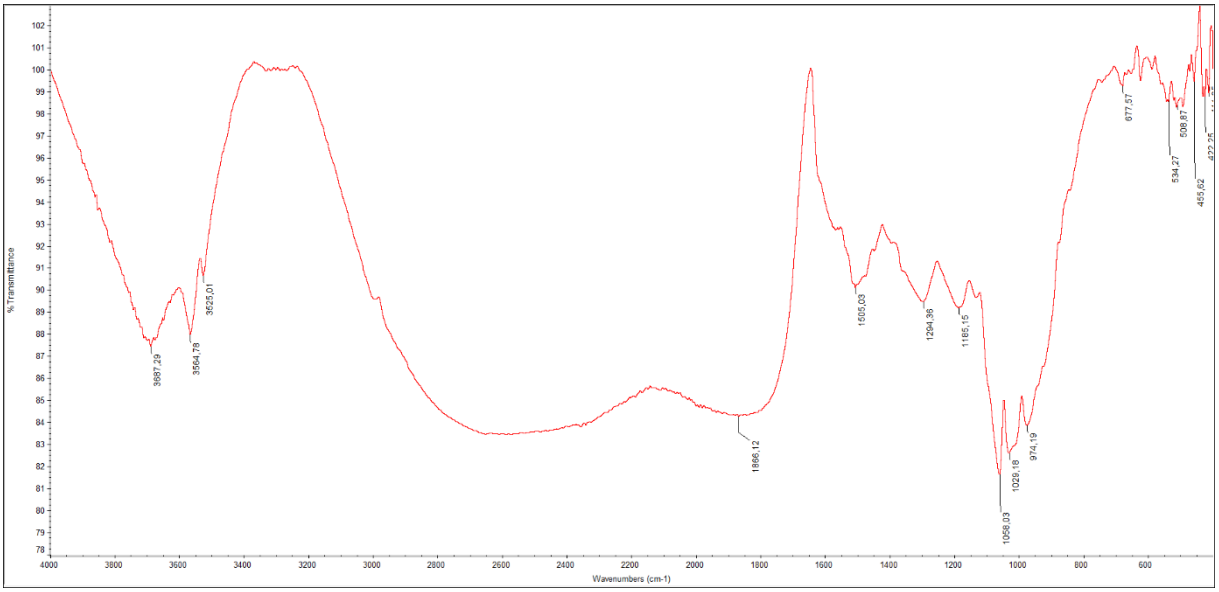

Figure 1. FTIR-ATR spectrum of PEDOT/ERGO prepared in 0.1 M $LiClO_4$/ACN

FTIR spectroscopic measurement was given in Figure 1. The vibrational bands at 1555 cm^{-1} and 1294 cm^{-1} in the FTIR spectrum of PEDOT are ascribed to the C=C and C–C stretching vibrations of the quinonoid structure and thiophene rings, respectively. The C–O–C bending vibration in the ethylenedioxy group corresponds to the bands at 1185, 1058, and 1029 cm^{-1}. It is observed that the C-

S stretching vibration in thiophene rings is responsible for the bands at 974 and 677 cm^{-1}, corroborating the formation of PEDOT network.

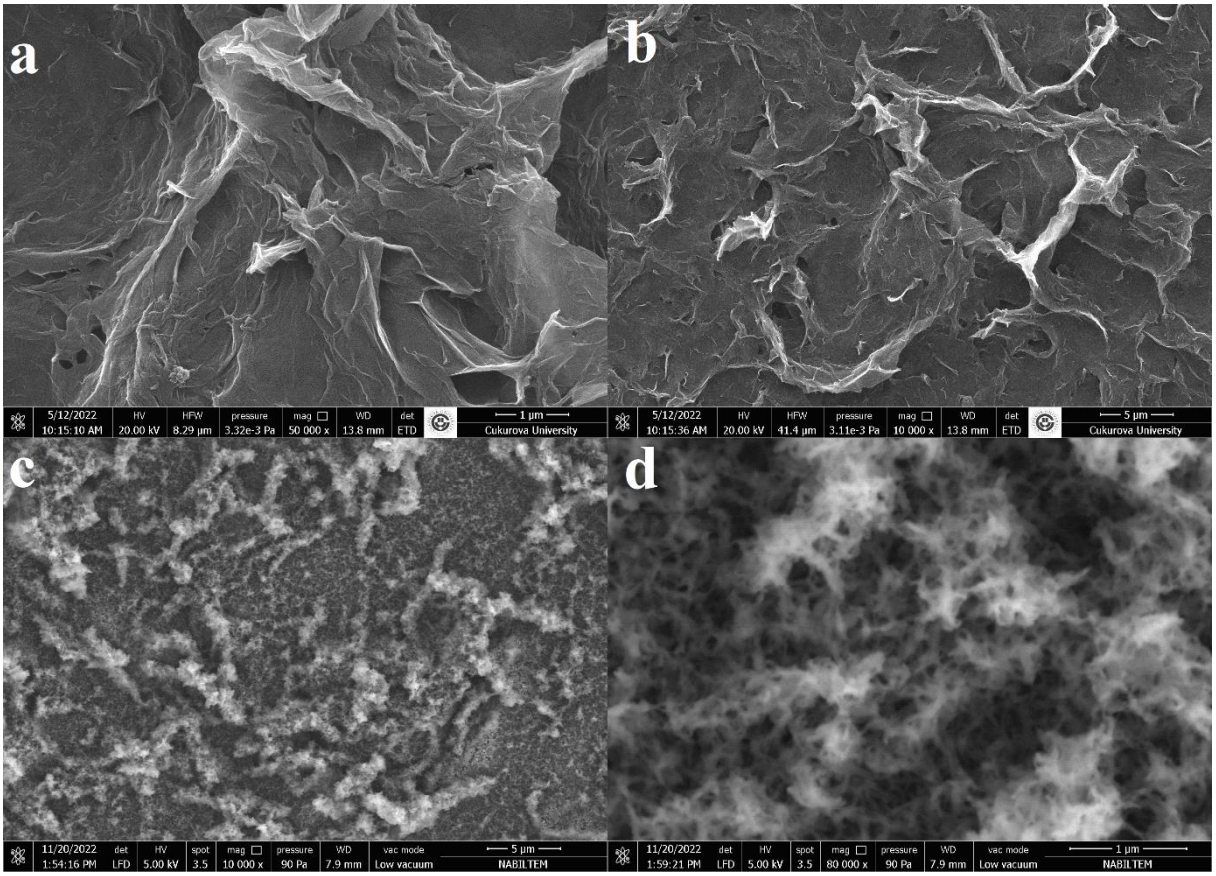

Figure 2. SEM images of ERGO given in different magnifications (a and b), PEDOT/ERGO prepared in 0.1 M $LiClO_4$/ACN given in different magnification (c and d).

Figures 2a and 2b display the ERGO SEM picture at various magnifications. The surface structures of ERGO presents a uniformly wavy and wrinkled sheet structure. Figures 2c and d show electro-coated PEDOT prepared in 0,1 M $LiClO_4$/ACN presenting rough and porous network PEDOT architectures indicating the surface of ERGO homogeneously covered by PEDOT.

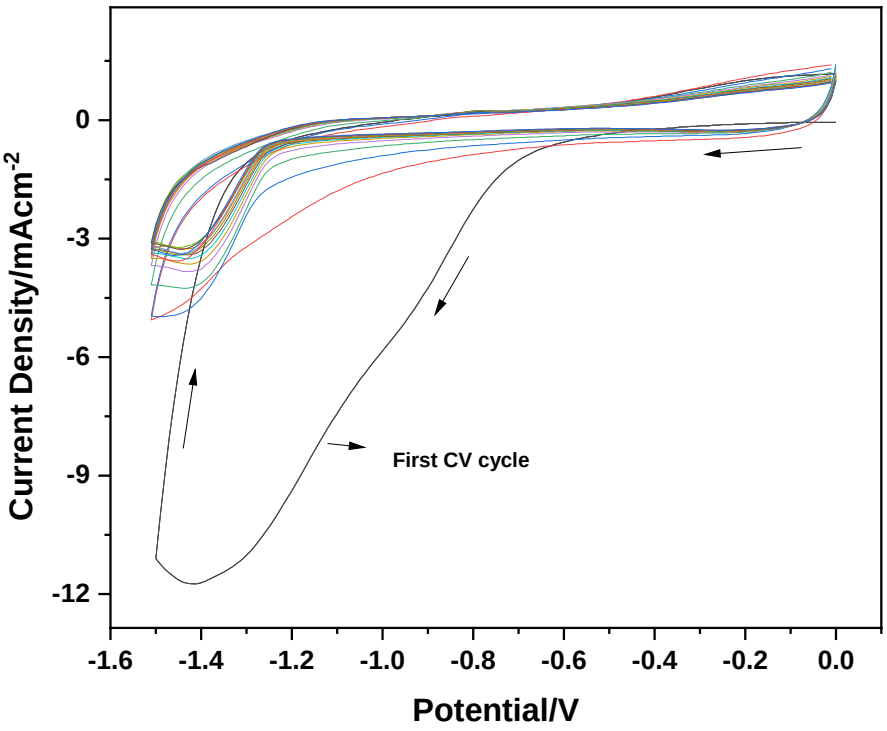

Figure 3. Cyclic voltammograms of GO/GCE electrode in 0.1 M pH=7.0 phosphate buffer saline performed at a scan rate of 50 mV/s subjected to 15 cycles in the potential range from 0 to -1.5 V.

GO is not conductive to electricity because of the high concentration of oxygen functions on the carbon's basal planes (Toh, et al., 2014). In order to make GO electrically conductive, the material must first be deoxygenated via an electrochemical process. Using a scan rate of 50 mVs^{-1} in a 0.1 M pH = 7.0 PBS solution, GO was electrochemically reduced by cycling through a potential range of 0 to -1.5 V during 15 consecutive cycle (Figure 3). After 15 cycles of the first cathodic scan, it is determined that, a drop in oxygen moieties at the GO basal plane is responsible for a considerable decrease in the current density of a huge cathodic peak centered at -1.4 V.

Three different electrolyte solutions (0.1M Et_4NBF_4/ACN, Bu_4NPF_6/ACN, and $LiClO_4$/ACN) containing 10 mM EDOT were used to electrodeposit the PEDOT onto ERGO/GCE. Figure 4 depicts the effect of electrolyte on electrochemical polymerization of PEDOT deposited on ERGO/GCE. The sequence of PF_6^- > ClO_4^- > BF_4^- determines the PEDOT polymerization behavior, which is dependent on the electrolyte type. The kind of anion has an impact on the polymerization effectiveness, which is consistent with polymerization of thiophene (Schrebler, et al., 1997). The increased integral area for the PF_6^- anion is an indicative of a rise in oligomer formation, therefore, more polymerization efficiency. Therefore, an increased current density is observed in the case of the PF_6^- anion when compared to the BF_4^- and ClO_4^- anions, attributed to the stronger alkaline nature of PF_6^-anion,

facilitating the loss of H^+ during the polymerization process. (Sarac, et al., 2022). EDOT oxidation in 0.1 M Bu_4NPF_6, $LiClO_4$, Et_4NBF_4/ACN began at 1.34, 1.30, and 1.25 V, respectively, which supposes that the oxidation of EDOT monomer in various electrolyte systems differs significantly. On ERGO/GCE electrode, cyclic voltammograms of 10 mM initial monomer concentration of EDOT show that current density increased with each cycle, with anodic peak (E_{pa}) = 0.17 V, cathodic peak (E_{pc}) = -0.54 V for Bu_4NPF_6, E_{pa} = 0.22 V, E_{pc} = -0.51 V for Et_4NBF_4, E_{pa} = 0.19 V, and V, E_{pc} = -0.28 V for $LiClO_4$. Figure 4b compares the PEDOT prepared in Et_4NBF_4/ACN without ERGO. ERGO may improve the diffusion of ions from the electrolyte by getting access to virtually all existing holes on the electrode, resulting in greater polymerization efficiency than PEDOT deposited on GCE without ERGO (El-Hallag, et al., 2019). As seen from Figure 4 b, polymerization efficiency of PEDOT deposited on GCE is lower than that of PEDOT deposited on ERGO/GCE.

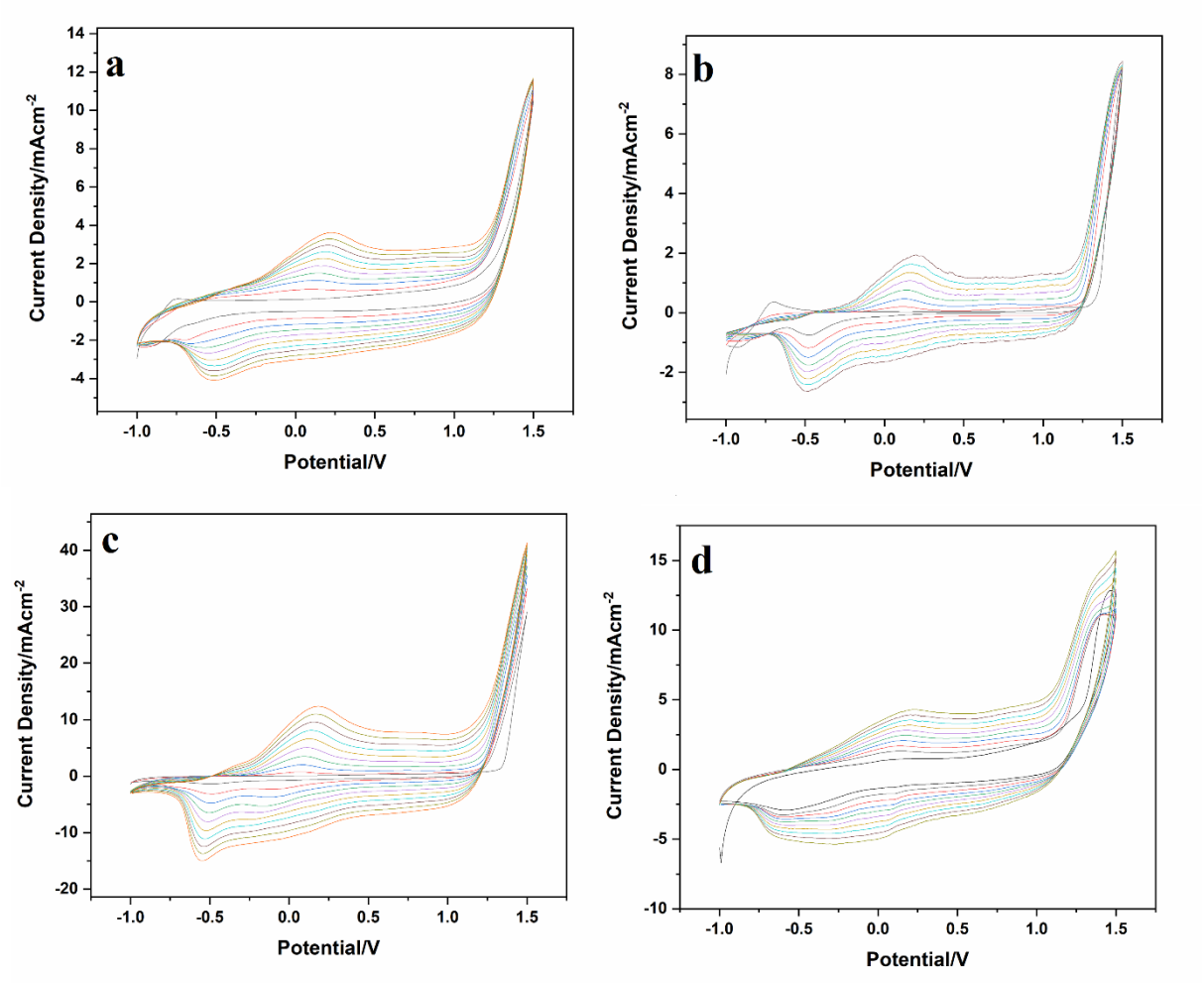

Figure 4. Cyclic voltammograms of growth of PEDOT on ERGO/GCE electrodes in (a) 0.1 M Et_4NBF_4/ACN, (b) cyclic voltammograms of growth of without ERGO on GCE in 0.1 M Et_4NBF_4/ACN, (c) 0.1 M Bu_4NPF_6/ACN, (d) 0.1 M $LiClO_4$/ACN at a scan rate of 100 mV/s subjected to 10 cycles in the potential range from -1.0 to 1.5 V.

Figures 5 a-c show cyclic voltammograms of PEDOT/ERGO in various electrolytes at scan rates between 10 mVs^{-1} and 100 mVs^{-1} in 0.1M Et_4NBF_4/ACN, Bu_4NPF_6/ACN, and $LiClO_4$/ACN. Because of how polarization and diffusion work together, the shape of the CV waveform changes depending on the type of electrolyte. This suggests that the process is irreversible and very complicated. Differences in peak potential (E_p) are not minor, and they are caused by the behavior of electrolyte ion diffusion. (Karazehir, et al., 2021). The peak potential should be independent of the scan rate if diffusion is the main factor influencing a redox process. In order to learn more about the capacitive behavior of PEDOT/ERGO, a CV research was carried out at different scan speeds. The shapes of CV show a both rectangular box characteristic and pseudocapacitive characteristic due to faradaic reaction of PEDOT. Anodic and cathodic redox peaks in cyclic voltammogram are clearly observed, that typically arises from pseudo type capacitive behavior of PEDOT, located at E_{pa}=-0.58 V, E_{pc}=-0.74 V for Bu_4NPF_6, E_{pa}=0.3 V, E_{pc}=-0.5 V for Et_4NBF_4, and E_{pa}=0.1 V, E_{pc}=-0.58 V for $LiClO_4$, where positive shift observed at anodic oxidation peak potential of PEDOT following order Bu_4NPF_6, Et_4NBF_4, $LiClO_4$.

The peak currents (I_p) against the square root of the scan rate (Figure 5d) are used to characterize the scan rate dependence of the polymer-coated electrodes. Thus, the polymers show a good correlation coefficient (R between 0.99 and 0.95) between I_p and the square root of the scan rate, suggesting a diffusion-limited process.

The Randles–Sevcik equation at room temperature is given as:

$$i_p = 268600n^{3/2}ACD^{1/2}\vartheta^{1/2} \quad (1)$$

Here i_p (A) is the maximum current density, the number of electrons n (=1) transferred in the redox reaction, A the electrode area (0.07 cm^2), D (cm^2s^{-1}) the diffusion coefficient, C the concentration of the diffusing species ($molcm^{-3}$), and υ (Vs^{-1}) the scan rate. Diffusion coefficient of electrolytes from anodic lines can be determined slope of graph given in Figure 5d. The diffusion coefficient is calculated to be $1.27x10^{-4}$ cm^2s^{-1} for $LiClO_4$, $9.84x10^{-5}$ cm^2s^{-1} for Et_4NBF_4, and $8.23x10^{-5}$ cm^2s^{-1} for Bu_4NPF_6.

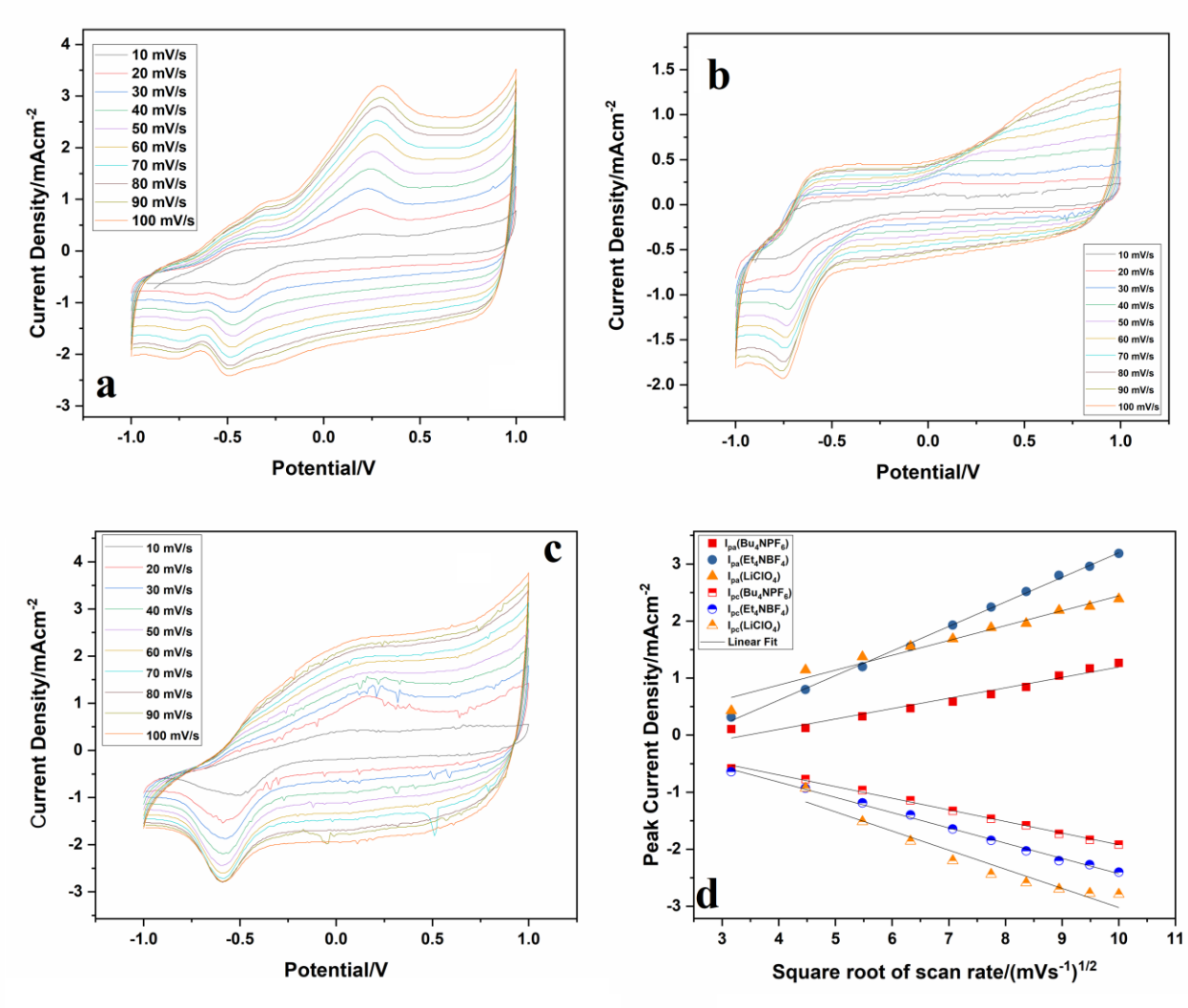

Figure 5. Cyclic voltammograms of PEDOT/ERGO in (a) 0.1 M Et_4NBF_4/ACN, (b) 0.1 Bu_4NPF_6/ACN, 0.1 M $LiClO_4$/ACN, at various scan rates from 10 mVs^{-1} to 100 mVs^{-1}, (d) the square root of scan rates vs peak current density.

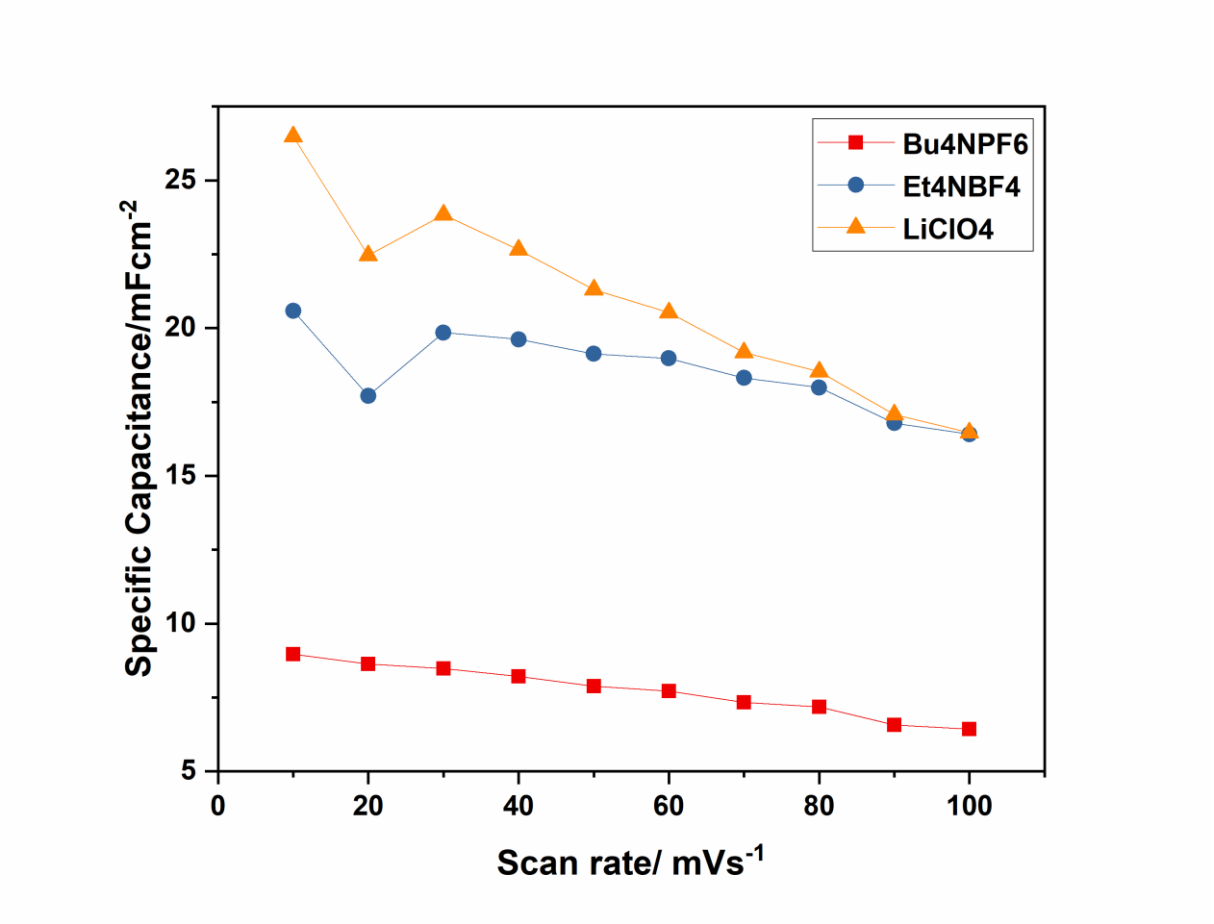

Figure 6. C_{sp} of PEDOT/ERGO at different scan rates and in different electrolyte solutions.

The specific capacitance (C_{sp}) value of the PEDOT/ERGO electrodes were estimated from CV data according to Eqn. 2

$$C_{sp}=\frac{\int i d\upsilon}{2As\Delta V} \quad (2)$$

where, $\int i d\upsilon$ is the entire integral area of the CV curve, A is the geometric area of electrode (cm^2), s is the scan rate (Vs^{-1}), and ΔV is the applied potential window (V) of the CV curve. Figure 6 shows the plot of scan rate vs. C_{sp} of PEDOT/ERGO coated GCE prepared in different electrolyte solutions. C_{sp} values drop as the scan rate increases. A drop in C_{sp} may be related to the inability of electrolyte ions to permeate entirely through surface of the electrode at faster scan speeds, since the electrolyte ions can only reach the outermost layers of the electrode (Ismar, et al., 2018). C_{sp} for PEDOT/ERGO increases in the following order Bu_4NPF_6, Et_4NBF_4 and $LiClO_4$. Lower scan speeds are more advantageous for larger store capacity. At low scan rates of 10 mVs^{-1}, the maximum specific capacitance (C_{sp}) of the PEDOT/ERGO electrode is estimated to be 8.96 $mFcm^{-2}$ for 0.1 M Bu_4NPF_6/ACN, 20.58 $mFcm^{-2}$ for 0.1 M Et_4NBF_4/ACN, and 26.48 $mFcm^{-2}$ for 0.1 M $LiClO_4$/ACN. The C_{sp} found for PEDOT/ERGO prepared in 0.1 M $LiClO_4$/ACN is significantly greater than the areal capacitance values published for various nanostructured electrode systems for supercapacitors

such as CdSe-8h (1.285 $mFcm^{-2}$ at 10 mVs^{-1}) (Pawar, et al., 2017), α-$Co(OH)_2$/f-GNS (2.108 $mFcm^{-2}$ at 10 mVs^{-1}) (Jin, etal., 2017), TiO_2 nanotube array (Ar-S1) (13.26 $mFcm^{-2}$ at 20 mVs^{-1}) (Raj et al., 2020), and on the other hand, the areal capacitance values reported here are comparable to that of r-TNAS (24.07 $mFcm^{-2}$ at 10 mVs^{-1}) (Li et al., 2015).

Galvanostatic charge and discharge test (GCD) was applied to determine the specific capacitance, as well. C_{sp} was calculated according to eqn 3.

$$Csp = \frac{I\Delta t}{\Delta V A} \quad (3)$$

where, I is the applied current (A), Δt is the discharge time (s), ΔV is the applied potential window (V) of the GCD curve and A is the geometric area of electrode (cm^2). Figures 7 a-c show the GCD curves of prepared PEDOT/ERGO electrodes in various electrolytes. As seen from Figures 7 a-c, The C_{sp} decreases with increasing current density. GCD curve correlates the voltametric measurements, where the highest C_{sp} obtained for PEDOT/ERGO film prepared in 0.1 M $LiClO_4$/ACN. The maximum C_{sp} of the PEDOT/ERGO electrode at 0.1 $mAcm^{-2}$ is calculated to be 6.1 $mFcm^{-2}$ for 0.1 M Bu_4NPF_6/ACN, 17.5 $mFcm^{-2}$ for 0.1 M Et_4NBF_4/ACN, and 22.2 $mFcm^{-2}$ for 0.1 M $LiClO_4$/ACN (Figure 7 d).

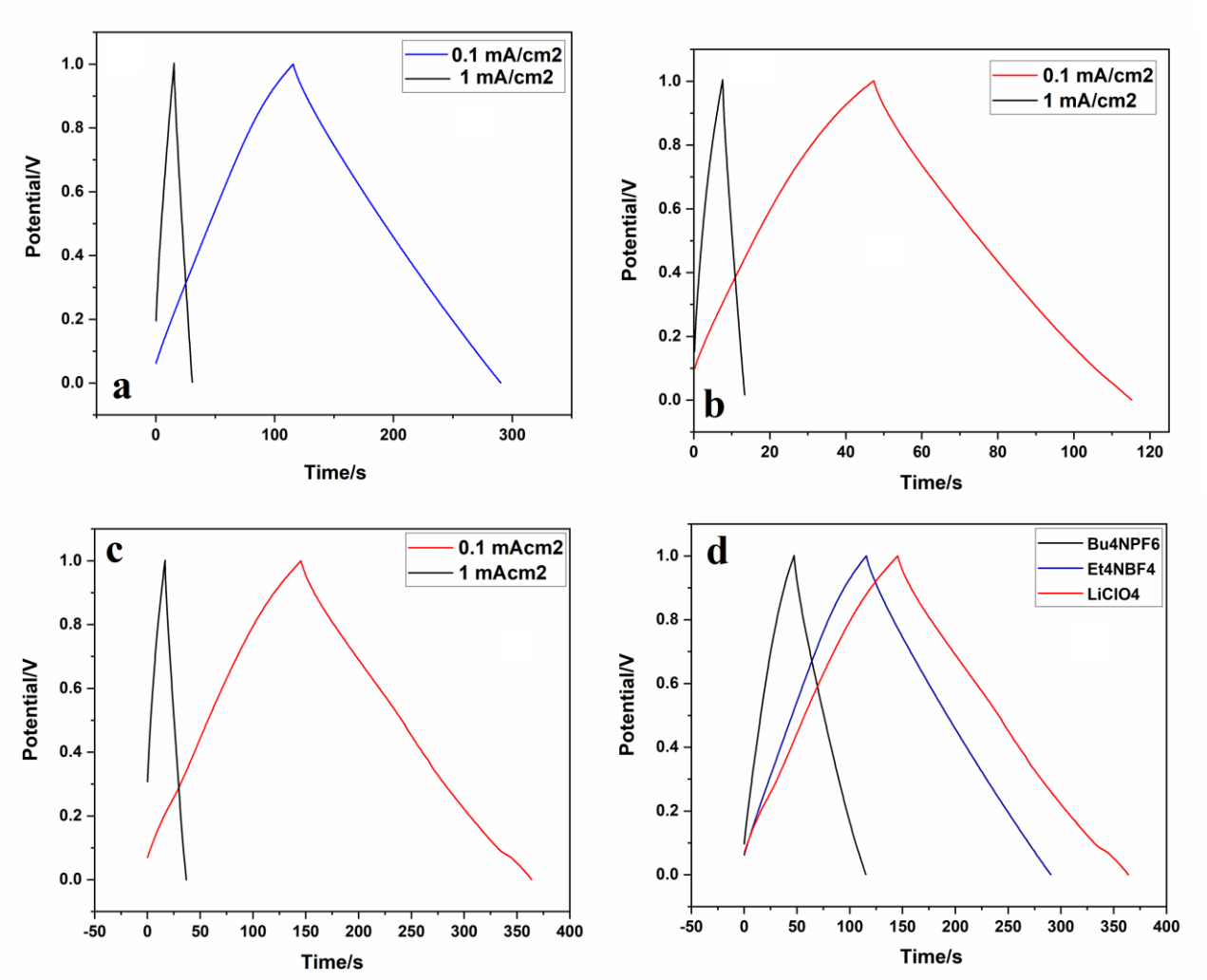

Figure 7. Galvanostatic charge discharge (GCD) curve with respect to two different current densities (0.1 $mAcm^{-2}$ and 1 $mAcm^{-2}$) PEDOT/ERGO electrodes in (a) 0.1 M Et_4NBF_4/ACN, (b) 0.1 M Bu_4NPF_6/ACN, (c) 0.1 M $LiClO_4$/ACN, (d) comparison of GCD of PEDOT/ERGO electrodes at a fixed 0.1 $mAcm^{-2}$ in 0.1 M Bu_4NPF_6/ACN, 0.1 M Et_4NBF_4/ACN, and 0.1 M $LiClO_4$/ACN.

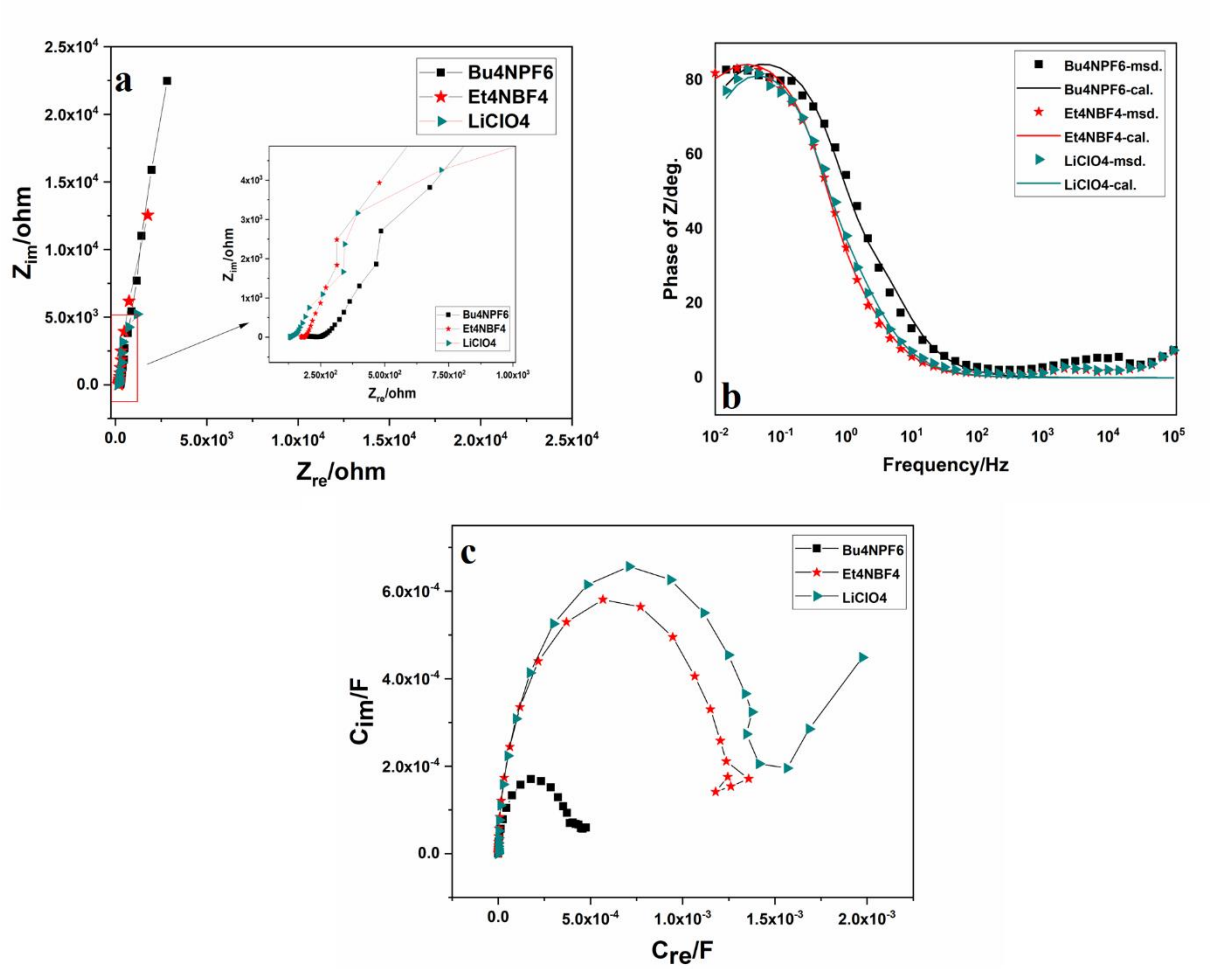

Figure 8 (a) Nyquist plots of PEDOT/ERGO electrodes, (b) Bode phase plots of PEDOT/ERGO electrodes, solid lines show calculated impedance data according to R(C(R(CR))) equivalent circuit, and (c) complex capacitance plots of PEDOT/ERGO electrodes.

Additionally, an EIS was conducted to examine the capacitive properties of the PEDOT/ERGO electrodes. Figure 8a presents the Nyquist plots for three distinct electrolytes. In the high-frequency range, solution resistance (R_s), also known as equivalent series resistance (ESR), is generated by the intercept at the real section of the axis. As the slope of the line in the low-frequency domain increases, the electrodes of a supercapacitor approach their optimal behavior. However, the deviation of nonideal capacitance behavior is shown by a line that is tilted (at an angle less than 90 degrees) toward the real axis. Figure 8b presents the Bode phase plots of PEDOT/ERGO electrodes. The phase angle at 0.01 Hz for the PEDOT/ERGO electrode is attained at 82.81^o for Bu_4NPF_6, 81.96^o for Et_4NBF_4, and 77.20^o for $LiClO_4$, indicating a deviation from ideal capacitive behavior evident with CV measurements due to the lack of an ideal rectangular CV shape. Experimental impedance data can be represented as complex capacitance plot for a more insightful depiction. Figure 8c shows the complex capacitance plots of PEDOT/ERGO electrodes in three different electrolytes. The real capacitance (C_{re}) for PEDOT/ERGO electrodes at a low frequency of 10 mHz is observed to be 28.14 $mFcm^{-2}$ for $LiClO_4$,

17.86 $mFcm^{-2}$ for Et_4NBF_4, and 6.77 $mFcm^{-2}$ for Bu_4NPF_6, corroborating the voltametric and GCD measurements.

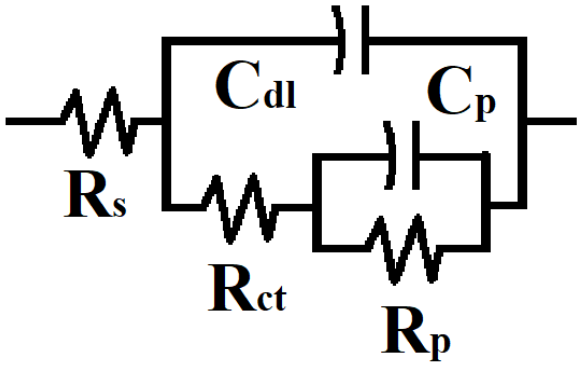

Figure 9. R(C(R(CR))) equivalent circuit used to fit experimental impedance measurements

To fit the impedance diagram, the equivalent circuit model of R(C(R(CR))) was employed (Figure 9). The parameters of the R(C(R(CR))) circuit are shown in Table 1. The intercept at the real section of the axis produces solution resistance (Rs), often referred to as equivalent series resistance (ESR), at high frequencies. This resistance is a reflection of the electrolyte's ionic resistance, the contact resistance between the active material and the current collector, and the inherent resistance of the active materials. Increasing ionic conductivity of the electrolyte is reflected in the ESR, which were 16.38 Ωcm^2 for the PEDOT/ERGO electrode prepared in 0.1 M Bu_4NPF_6/ACN, 12.66 Ωcm^2 for prepared in Et_4BF_4/ACN, 9.49 Ωcm^2 for prepared in LiClO4/ACN. The highest C_{dl} and the lowest R_{ct} are observed for PEDOT/ERGO prepared in 0.1 M $LiClO_4$/ACN electrolyte, which are 13.70 $mFcm^{-2}$ and 18.75 Ωcm^2, respectively. C_p and R_p are attributed polymer film capacitance and resistance. As seen from table 1, the C_p increases from Bu_4NPF_6 to $LiClO_4$, whereas the R_p decreases in the same order.

Table 1. R(C(R(CR))) equivalent circuit parameters

PEDOT/ERGO	Bu_4NPF_6	Et_4NBF_4	$LiClO_4$
$R_s/\Omega cm^2$	16.38	12.66	9.49
$C_{dl}/mFcm^{-2}$	3.14	11.8	13.70
$R_{ct}/\Omega cm^2$	34.60	22.19	18.75
$C_p/mFcm^{-2}$	2.82	6.05	7.87
$R_p/k\Omega cm^2$	9.72	5.88	2.09
Chi squared/$\chi 2$	$7.74x10^{-3}$	$2.03x10^{-3}$	$4.70x10^{-3}$

4.Conclusion

PEDOT/ERGO electrodes for supercapacitor via a facile electrochemical method were fabricated. PEDOT/ERGO electrodes were evaluated by CV, GCD, and EIS tests. Capacitance values of PEDOT/ERGO electrodes are found to vary significantly depending on electrolyte type. PEDOT/ERGO produced in 0.1 M $LiClO_4$/ACN electrolyte solution also exhibits the highest specific capacitance and the lowest charge transfer resitance. Maximum specific capacitance is recorded as $C_{sp} = 26.48$ $mFcm^{-2}$ and specific capacitance values varies between $C_{sp} = 8.96–26.48$ $mFcm^{-2}$ for different electrolyte types at 10 mVs^{-1}. Thus, PEDOT/ERGO can be efficiently used for supercapacitor applications.

Statement of Conflict of Interest

Author has declared no conflict of interest.

Author's Contributions

The contribution of the author is 100%.

References

Ahmed S., Rafat M. Hydrothermal synthesis of PEDOT/rGO composite for supercapacitor applications. Materials Research Express 2018; 5(1): 015507.

Albadi MH., El-Saadany EF. Overview of wind power intermittency impacts on power systems. Electric Power Systems Research 2009; 80(6): 627-632.

Arbizzani C., Mastragostino M., Meneghello L. Polymer-based redox supercapacitors: A comparative study. Electrochimica Acta 1996; 41(1): 21-26.

Athira AR., Vimuna VM., Vidya K., Xavier TS. Nanotubular polyaniline electrode for supercapacitor application. 2nd International Conference on Condensed Matter and Applied Physics (ICC), Nov 24-25 2017, Page number: 1-4, Bikaner.

Bang K., Im KI., Kim DG., Park SH., Chung EY. Power Failure Protection Scheme for Reliable High-Performance Solid State Disks. Ieice Transactions on Information and Systems 2013; E96D(5): 1078-1085.

Cairns EJ., Albertus P. Batteries for Electric and Hybrid-Electric Vehicles. Annual Review of Chemical and Biomolecular Engineering, 2010; 1: 299-320.

Choudhary MK., Sharma AK., Integration of PV, Battery and supercapacitor in islanded microgrid. 1st International Conference on Emerging Frontiers in Electrical and Electronic Technologies (ICEFEET), Jul 10-11 2020, Page number: 1-6, Patna.

El-Hallag IS., El-Nahass MN., Youssry SM., Kumar R., Abdel-Galeil MM., Matsuda A. Facile in-situ simultaneous electrochemical reduction and deposition of reduced graphene oxide embedded palladium nanoparticles as high performance electrode materials for supercapacitor with excellent rate capability. Electrochimica Acta 2019; 314: 124-134.

Hashim MA., Yatim NM., Mahmud NA., Sazali C., Hamdan NES.,Yahya E., Ngah MA., Suhaimi S. Hybrid solid polymer electrolyte from diapers as separator for electrochemical double layer Capacitor (EDLC), International Conference on Recent Advancements in Science and Technology (ICoRAST), Nov 07-08 2017, Page number: 1-10, Melaka.

Hu YH., Schlipf J., Wussler M., Petrus ML., Jaegermann W., Bein T., Muller-Buschbaum P., Docampo P. Hybrid Perovskite/Perovskite Heterojunction Solar Cells. ACS Nano 2016; 10(6): 5999-6007.

Hu ZX., Zhang XY., Gao M., Zhou HW., Wu MX. PEDOT@4A-Molecular Sieve Composite Electrode for Supercapacitor. Physica Status Solidi a-Applications and Materials Science 2019; 216:1900188.

Huang ZQ., Guo HL., Zhang C. Assembly of 2D graphene sheets and 3D carbon nanospheres into flexible composite electrodes for high-performance supercapacitors. Composites Communications 2019; 12: 117-122.

Huet F., Boitier V., Seguier L. Tunable Piezoelectric Vibration Energy Harvester With Supercapacitors for WSN in an Industrial Environment. Ieee Sensors Journal 2022; 22(15): 15373-15384.

Ismar E., Karazehir T., Ates M., Sarac AS. Electrospun carbon nanofiber web electrode: Supercapacitor behavior in various electrolytes. Journal of Applied Polymer Science 2018; 135(4); 45723.

Jiang YQ., Wang PB., Zang XN., Yang Y., Kozinda A., Lin LW. Uniformly Embedded Metal Oxide Nanoparticles in Vertically Aligned Carbon Nanotube Forests as Pseudocapacitor Electrodes for Enhanced Energy Storage. Nano Letters 2013; 13(8): 3524-3530.

Jin EM., Lee HJ., Jun HB., Jeong SM. Electrochemical properties of alpha-Co(OH)(2)/graphene nano-flake thin film for use as a hybrid supercapacitor. Korean Journal of Chemical Engineering 2017; *34*(3): 885-891.

Karazehir T., Sarac B., Gilsing HD., Gumrukcu S., Eckert J., Sarac A. S. Functionalized highly electron-rich redox-active electropolymerized 3,4-propylenedioxythiophenes as precursors and targets for bioelectronics and supercapacitors. Molecular Systems Design and Engineering 2021: 6(3), 214-233.

Landers M., Elhadad A., Rezaie M., Choi S. Integrated Papertronic Techniques: Highly Customizable Resistor, Supercapacitor, and Transistor Circuitry on a Single Sheet of Paper. ACS Applied Materials & Interfaces 2022; 14(40): 45658-45668.

Li Z., Ding YT., Kang WJ., Li C., Lin D., Wang XY., Pan DY Reduction Mechanism and Capacitive Properties of Highly Electrochemically Reduced TiO2 Nanotube Arrays. Electrochimica Acta 2015; 161: 40-47.

Liu J., Yang Q., Li MZ., Zhu WH., Tian H., Song YL. Organic dye-sensitized sponge-like TiO_2 photoanode for dye-sensitized solar cells. Philosophical Transactions of the Royal Society a-Mathematical Physical and Engineering Sciences 2013; 371: 20120314.

Liu XY., Huang WL., Wang DD., Tian JH., Shan ZQ. A nitrogen-doped 3D hierarchical carbon/sulfur composite for advanced lithium sulfur batteries. Journal of Power Sources 2017; 355: 211-218.

Meroni SMP., Mouhamad Y., De Rossi F., Pockett A., Baker J., Escalante R., Searle J., Carnie MJ., Jewell E., Oskam G., Watson TM. Homogeneous and highly controlled deposition of low viscosity inks and application on fully printable perovskite solar cells. Science and Technology of Advanced Materials 2018; 19(1): 1-9.

Murugan AV., Quintin M., Delville MH., Campet G., Gopinath CS., Vijayamohanan K. Exfoliation-induced nanoribbon formation of poly(3,4-ethylene dioxythiophene) PEDOT between MoS_2 layers as cathode material for lithium batteries. Journal of Power Sources 2006; 156(2): 615-619.

Naoi K., Naoi W., Aoyagi S., Miyamoto J., Kamino T. New Generation "Nanohybrid Supercapacitor". Accounts of Chemical Research 2013; 46(5): 1075-1083.

Nelson RF., Power requirements for batteries in hybrid electric vehicles. Journal of Power Source 2000; 91(1): 2-26.

Pawar SA., Patil DS., Shin JC. Cadmium selenide microspheres as an electrochemical supercapacitor. Materials Today Chemistry 2017; *4*: 164-171.

Raj CC., Srimurugan V., Flamina A., Prasanth R. Tuning the carrier density of TiO2 nanotube arrays by controlling the oxygen vacancies for improved areal capacitance in supercapacitor applications. Materials Chemistry and Physics 2020; 248: 122925

Ranjan S., Balaji S., Panella RA., Ydstie BE. Silicon solar cell production. Computers & Chemical Engineering 2011; 35(8): 1439-1453.

Raza W., Ali FZ., Raza N., Luo YW., Kim KH., Yang JH., Kumar S., Mehmood A., Kwon EE. Recent advancements in supercapacitor technology. Nano Energy 2018; 52: 441-473.

Ryu KS., Lee YG., Hong YS., Park YJ., Wu XL., Kim KM., Kang MG., Park NG., Chang SH. Poly(ethylenedioxythiophene) (PEDOT) as polymer electrode in redox supercapacitor. Electrochimica Acta 2004; 50(2-3): 843-847

Safari B. Modeling wind speed and wind power distributions in Rwanda. Renewable & Sustainable Energy Reviews 2011; 15(2): 925-935.

Sarac B., Karazehir T., Gilsing HD., Eckert J., Sarac AS. Effect of supporting electrolyte on capacitance and morphology of electrodeposited poly(3,4-propylenedioxythiophene) derivatives bearing reactive functional groups. Molecular Systems Design and Engineering 2022; 7(5); 460-479.

Schrebler R., Grez P., Cury P., Veas C., Merino M., Gomez H., Cordova R., del Valle MA. Nucleation and growth mechanisms of poly(thiophene) - Part 1. Effect of electrolyte and monomer concentration in dichloromethane. Journal of Electroanalytical Chemistry 1997; 430(1-2); 77-90.

Smith TA., Mars JP., Turner GA.. Using supercapacitors to improve battery performance, 33rd IEEE Annual Power Electronics Specialists Conference (PESC02), Jun 23-27 2002, page number:124-128, Carins.

Snook GA., Kao P., Best AS. Conducting-polymer-based supercapacitor devices and electrodes. Journal of Power Sources 2011; 196(1): 1-12.

Sonia TS., Mini PA., Nandhini R., Sujith K., Avinash B., Nair S.V., Subramanian KRV. Composite supercapacitor electrodes made of activated carbon/PEDOT:PSS and activated carbon/doped PEDOT. Bulletin of Materials Science 2013; 36(4), 547-551.

Su DS. Batteries/Supercapacitors: Hybrids with CNTs. Nanocarbon- Inorganic Hybrids: Next Generation Composites for Sustainable Energy Applications. Berlin: Walter de Gruyter GmbH; 2014.

Toh SY., Loh KS., Kamarudin SK., Daud WRW. Graphene production via electrochemical reduction of graphene oxide: Synthesis and characterisation. Chemical Engineering Journal 2014; 251: 422-434.

Vonlanthen D., Lazarev P., See KA., Wudl F., Heeger AJA. Stable Polyaniline-Benzoquinone-Hydroquinone Supercapacitor. Advanced Materials 2014; 26(30): 5095-5100.

Wang CG., Zhou E., He WD., Deng XL., Huang JZ., Ding M., Wei XQ., Liu XJ., Xu XJ. $NiCo_2O_4$-Based Supercapacitor Nanomaterials. Nanomaterials 2017; 7(2): 41.

Wang XB., Zhao Y., Wu FC., Liu SM., Zhang ZS., Tan ZY., Du XH., Li JD. ZIF-7@carbon composites as multifunctional interlayer for rapid and durable Li-S performance. Journal of Energy Chemistry 2021; 57: 19-27.

Wang Y., Mayorga-Martinez CC., Pumera M. Polyaniline/MoSX Supercapacitor by Electrodeposition. Bulletin of the Chemical Society of Japan 2017; 90(7): 847-853.

Xu JJ., Zhou S. Research on the target power level for Li-air battery and weight ratio distribution in a dual-battery vehicle system with Li-ion battery, International Conference on Intelligent Systems Research and Mechatronics Engineering (ISRME), Apr 11-13 2015, page number:1199-1205, Zhengzhou.

Yang W, Ni M., Ren X., Tian YF., Li N., Su YF.,Zhang XL. Graphene in Supercapacitor Applications. Current Opinion in Colloid & Interface Science 2015; 20(5-6): 416-428.